Infrared spectroscopic study of rovibrational states of methane trapped in parahydrogen crystal

Takamasa Momose,[a] Masaaki Miki, Tomonari Wakabayashi, and Tadamasa Shida
Department of Chemistry, Graduate School of Science, Kyoto University, Kyoto 606-01, Japan

Man-Chor Chan,[b] Steven S. Lee, and Takeshi Oka
Department of Chemistry, The University of Chicago, Chicago, Illinois 60637

(Received 23 June 1997; accepted 15 August 1997)

The ν_3 and ν_4 vibrational transitions of methane trapped in solid parahydrogen have been observed by using Fourier transform infrared and high resolution laser spectroscopy. The observed spectrum is interpreted in terms of rovibrational states of the spherical rotor which are subjected to the crystal field splitting. The ν_4 band shows extremely sharp lines of a width of $\sim 0.003\ \mathrm{cm}^{-1}$, while the ν_3 band exhibits broader lines of a width of $1\ \mathrm{cm}^{-1}$. The infrared selection rules derived from an extended group theory to take into account the field effect are consistent with the observed spectra. The intermolecular interaction and the field effect in solid parahydrogen are analyzed quantitatively.
 [S0021-9606(97)04743-0]

I. INTRODUCTION

High resolution spectroscopy is generally regarded as not applicable to systems in condensed phase because of the spectral broadening due to strong intermolecular/atomic interactions.[1] However, a marked exception is found recently for parahydrogen crystal: Okumura *et al.* observed that an infrared spectral line of $W_0(0)$ transition (i.e., $v=0\leftarrow 0$, $J=6\leftarrow 0$) in a parahydrogen crystal shows a linewidth of only $0.006\ \mathrm{cm}^{-1}$ full width at half-maximum (FWHM)[2] In the wake of this pioneering work high resolution infrared absorption and stimulated Raman gain spectroscopic studies on solid parahydrogen have been made to reveal linewidths as narrow as $0.0003\ \mathrm{cm}^{-1}$ (Refs. 3–14). The narrow spectral linewidths originate in the weak intermolecular interaction in solid parahydrogen. Since the $J=0$ state proper to parahydrogen at cryogenic temperatures is spherically symmetric in charge density distribution, no averaged multipole exists and only the weak dispersion force assembles the molecules into a quantum solid.[15–17] Besides this feature, the extremely low density of states in solid parahydrogen provides an environment where the energy relaxation is very slow. The low density of states is, of course, attributed to the large vibrational and rotational molecular parameters of the hydrogen molecule.

Since the binding energy of solid parahydrogen is extremely weak, the neighboring intermolecular separation (3.783 Å) is distinctly larger than the interatomic separation of rare gas solids such as solid Ne (3.20 Å), etc. Also, the amplitude of the zero point vibration amounts to almost 20% of the intermolecular distance.[15] Owing to the weak intermolecular interaction and to the large intermolecular distance as well as to the large zero point vibration and the small mass of the constituent molecule, solid parahydrogen provides an ample and ''soft'' space for guest molecules. The softness allows guest molecules to undergo vibrational and rotational motions with little hindrance.

By virtue of these salient features the parahydrogen crystal can be utilized as an excellent matrix for matrix isolation spectroscopy. We have been utilizing the parahydrogen crystal as a new matrix in a series of papers.[18–22] Most of the observed infrared spectral bands of molecules trapped in solid parahydrogen are found to be sharper than those observed in conventional matrices by orders of magnitude. With sufficiently high resolution the vibrational and rotational motion of guest molecules as well as the host-guest interaction should be detectable spectroscopically. Thus, solid parahydrogen is a very promising substance for developing a new frontier of matrix isolation spectroscopy.

In the present work we have dealt with methane trapped in solid parahydrogen as the first step in vibration–rotation studies of molecules in the solid. The molecular rotation in solid phase was first discussed by Pauling in 1930[23] which led to spectroscopic studies of methane in rare gas matrices[24–26] and in solid nitrogen molecules.[27] However, the rotational motion of methane in these matrices is significantly hindered. Also, the existence of multiple trapping sites prevented detailed analysis of the infrared bands ν_3 and ν_4 of methane.[28–31] In contrast to these conventional matrices, solid parahydrogen may allow methane to rotate more freely because the van der Waals radius of methane of about 1.62 Å is distinctly smaller than the intermolecular distance of 3.783 Å of solid parahydrogen. Furthermore, since the parahydrogen crystal is a quantum solid, mechanical strain causing multiple trapping sites in nonquantum solids may not be developed in the crystal. Thus, methane in parahydrogen crystal should be ideal for the quantitative study of vibration and rotation of molecules in solids.

If the expected quasi-free vibration–rotation states are realized, the vibration–rotation energy states of methane in parahydrogen crystal should be classified by such an ex-

[a]Electronic mail: momose@kuchem.kyoto-u.ac.jp
[b]Present address: Department of Physics, Ibaraki University, Mito, Ibaraki 310, Japan.

tended group theory as developed by Miller and Decius.[32] In a separate article[33] (hereafter referred to as Article I), a theoretical framework for the analysis of the vibration–rotation of methane in parahydrogen crystal based on such group theory is worked out. In this article we will apply the theory to the analysis of the observed infrared spectra of methane in parahydrogen crystal.

Theoretical background discussed in Article I is briefly recapitulated in Sec. II. Experimental details and results are described in Secs. III and IV. The spectral analysis is made in Sec. V followed by discussion in Sec. VI.

II. THEORETICAL BACKGROUND

The crystal field potential, the symmetry classification of the rotational energy levels, and the optical selection rules are discussed extensively in Article I. Here, we briefly summarize the theory.

The first two anisotropic crystal field potential functions of solid parahydrogen acting on methane (designated as molecule 1) can be written as

$$V(\Omega_1)=\epsilon_{3c}V_3(\Omega_1)+\epsilon_{4c}V_4(\Omega_1), \tag{1}$$

where

$$V_3(\Omega)=\frac{1}{2}\,[D^{(3)}_{2,3}(\Omega)-D^{(3)}_{-2,3}(\Omega)+D^{(3)}_{2,-3}(\Omega) - D^{(3)}_{-2,-3}(\Omega)],$$

$$V_4(\Omega)=\frac{1}{2\sqrt{6}}\,\{\sqrt{5}[D^{(4)}_{4,0}(\Omega)+D^{(4)}_{-4,0}(\Omega)] + \sqrt{14}D^{(4)}_{0,0}(\Omega)\}.$$

The function $D^{(l)}_{k,m}(\Omega)$ is Wigner's rotation matrix whose definition and the rule of transformation of the function under rotation are given by Hougen.[34] The angle Ω represents the orientation of methane relative to the crystal c axis. The coefficients ϵ_{3c} and ϵ_{4c} are called crystal field parameters. The value of ϵ_{3c} is estimated to be $-19.24\ \mathrm{cm}^{-1}$ in Article I.[33]

The degeneracy of the rotational levels of methane is lifted in solid parahydrogen by the anisotropic crystal field. The split energy levels are classified according to the extended group G which is composed of the operations

$$\mathrm{G}=\{E\overline{E},8E\overline{(123)},3E\overline{(12)(34)},6\sigma_h\overline{(1234)^*},6\sigma_h\overline{(12)^*},$$
$$2C_3\overline{E},16C_3\overline{(123)},6C_3\overline{(12)(34)},12S_3\overline{(1234)^*},12S_3\overline{(12)^*},$$
$$3C_2\overline{E},24C_2\overline{(123)},9C_2\overline{(12)(34)},18\sigma_v\overline{(1234)^*},18\sigma_v\overline{(12)^*}\}. \tag{2}$$

The group G is a subgroup of the direct product group of the point group of the crystal symmetry (D_{3h}) and the permutation inversion group of methane (G_{24}). The group G is isomorphic to the direct product group of $D_3\otimes T_d$. In Eq. (2) the convention of Miller and Decius[32] putting bars on operations in molecular symmetry is followed. The symbol for each operation in the molecular symmetry is as follows: E-the identity operator; (123)-a cyclic permutation of identical particles; and (1234)*-a cyclic permutation accompanied by the space fixed inversion. The operations in the crystal symmetry without bars are written in standard point group notation,[35] where the C_3 axis is along the c axis of the crystal and the σ_h plane is in the hexagonal plane.

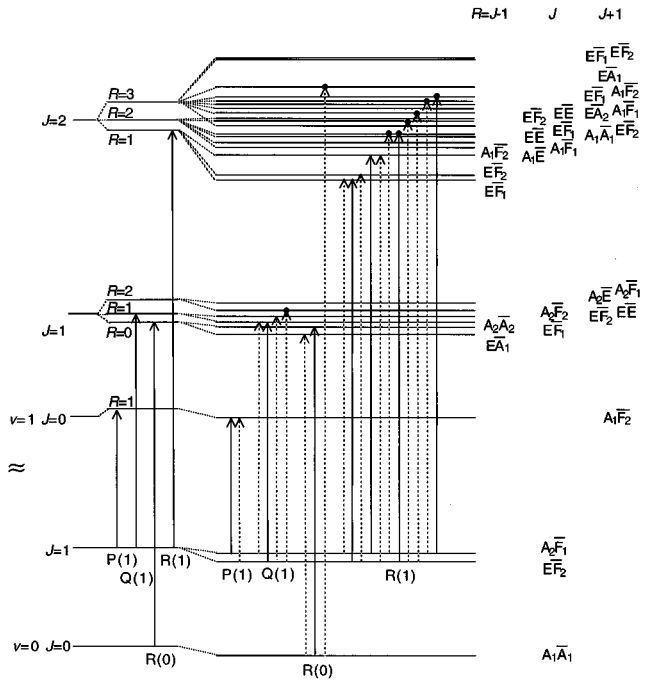

FIG. 1. The rovibrational levels of the ground vibrational $v=0$ (below the double wavy curves) and the ν_3 excited vibrational $v=1$ (above the curves) states. The energy levels denoted by J and R at the left-hand side are for the gas phase whereas those at the right-hand side labeled by the symbols $\Gamma\overline{\Gamma'}$ of the extended group G are for the crystal. The quantum number R is introduced to label the Coriolis-split triply degenerate vibrational state. It is suggested to refer to Tables V and VIII of Ref. 33 for easier association of the symbols $\Gamma\overline{\Gamma'}$ with the horizontal lines. The vertical solid arrows indicate the allowed transitions for radiation polarized parallel to the c axis while the dashed arrows indicate transitions polarized perpendicularly to the axis. The transitions of $\Delta R\neq 0$ are indicated by small full circles on the terminal levels.

Using the symmetry representation of the dipole moment in the laboratory fixed frame (A_2A_2 and EA_1), the selection rules for vibration–rotation transitions are obtained. In Fig. 1 the energy diagram of methane along with the symmetry classification, and the optical selection rules are depicted for $J=0$, 1 of the ground vibrational state and $J=0$, 1, 2 of the excited vibrational state. The solid and dashed arrows indicate, respectively, parallel and perpendicular transitions with respect to the c axis. Because the triply degenerate vibrational states of the ν_3 and ν_4 modes of methane are split by Coriolis coupling, the quantum number $R=J+\tilde{\ell}$ is appropriate to characterize the excited vibrational states where $\tilde{\ell}$ is the reversed vibrational angular momentum.[34,36]

As shown in Fig. 1, the P(1) transition in the crystal is predicted to consist of two components; the low frequency transition in the solid arrow is allowed for radiation polarized parallel to the c axis and the high frequency transition in the

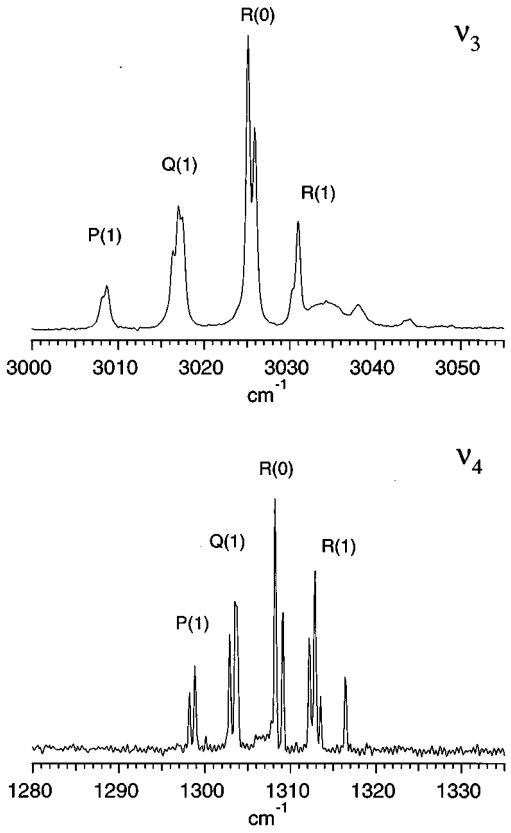

FIG. 2. FTIR spectra of methane trapped in solid parahydrogen. (a) The ν_3 fundamental band. (b) The ν_4 fundamental band. The spectral resolution is 0.25 cm^{-1}. The linewidths of the ν_3 and ν_4 transitions are about 1 cm^{-1} and 0.25 cm^{-1} (limit of the spectrometer), respectively.

dashed arrow for radiation polarized perpendicularly to the c axis. The Q(1) transition consists of four components. One is allowed for radiation parallel to the c-axis as shown in the solid arrow. Out of the remaining three the one ending at $v=1$, $J=1$, $R=2$ should be relatively weak because it is allowed only as a result of the breakdown of the angular momentum conservation due to the crystal field.[33] There are two components in the R(0) transition (both allowed transitions obeying the selection rule of $\Delta R=0$); the lower is perpendicular and the higher is parallel. The R(1) transitions shown on the right-hand side of Fig. 1 are more complicated. Here, the transitions between different R become allowed due to the mixing by the crystal field. As a result, a total of 11 transitions are possible for the R(1) transition. As will be discussed in connection with the experimental spectra shown in Fig. 2, the $\Delta R\neq 0$ ''forbidden'' transitions for the ν_4 mode are weaker than those for the ν_3 because of the larger Coriolis coupling in the former mode. The only observable $\Delta R\neq 0$ ''forbidden'' transition for the ν_4 mode is the transition of $J=1$, $R=2(EF_2)\leftarrow J=1(EF_2)$ which corresponds to the first arrow from the left among the transitions marked with solid full circles on the right-hand side of Fig. 1.

III. EXPERIMENT

Due to the relatively high vapor pressure of solid parahydrogen at cryogenic temperatures the usual technique of spraying matrix gases onto a cold surface in an open vacuum space is not applicable. We have grown a crystal of parahydrogen containing methane by slowly introducing the premixed gas into a closed cylindrical copper optical cell sealed by BaF_2 windows with indium gaskets. The i. d. and the path length of the optical cell is 1.7 and 3.0 cm, respectively. The cell is attached to the base of a Dewar type liquid helium cryostat equipped with a temperature controller stage. Parahydrogen gas is obtained by passing ultrahigh purity (>99.99995%) normal hydrogen gas through a column of hydrous ferric oxide orthopara converting catalyst (Ionex Research Corporation, Mesh Size 30×50) at 14–16 K. The impurity orthohydrogen concentration in the parahydrogen gas thus obtained is less than 0.1%. The mixed gas with a concentration of methane of 0.005%–0.01% is introduced continuously into the optical cell through a stainless steel tube. During this stage of sample growth the temperature of the cell is kept at around 7.2 K. Precise control of temperature as well as the gas flow rate are crucial to obtain a crystal with a good degree of isolation of methane. The crystal grows radially inward from the cylindrical copper wall. The crystal thus obtained is predominantly hexagonal close packed as proved by the stimulated Raman gain spectroscopy of $Q_1(0)$ transition.[8] The c axis of the crystal is along the direction of sample growth as optically demonstrated. The sample appears transparent which is advantageous for spectroscopic measurements.

Fourier transformed infrared (FTIR) spectra were recorded by a Nicolet FTIR spectrometer (Magna 750) with a resolution of 0.25 cm^{-1} and a Bomem FTIR spectrometer (DA-8) with a resolution of 0.01 cm^{-1}. A globar source, a CaF_2 or KBr beam splitter, and a liquid N_2 cooled HgCdTe (MCT) detector were used for the observation of the ν_3 and ν_4 bands of methane. The optical path was purged with N_2 gas to minimize the background absorption due to moisture in the air.

Difference frequency laser systems with a spectral purity better than 0.0001 cm^{-1} were used for the high resolution infrared laser spectroscopy of methane. The infrared radiation at the ν_3 band of methane (around 3025 cm^{-1}) was generated by getting difference frequencies between a single frequency of an Ar ion laser at 514.5 nm and frequencies of a ring dye laser at around 612 nm (Rhodamine 6G) in a temperature controlled $LiNbO_3$ of a size of $4\times 4\times 40$ mm.[37] The temperature of the crystal was tuned to achieve the phase matching. The temperature of the crystal was kept at about 370 °C by a home-built oven with a stability of ± 0.1 °C. The infrared radiation was detected by a liquid N_2 cooled InSb detector. The output power of the difference frequency infrared radiation was more than 100 μW when pumped by two equal-power beams of a total power of 1 W focused by a 25 cm focal length lens.

The infrared radiation at the ν_4 band of methane around 1308 cm^{-1} was generated by taking difference frequencies between two ring dye laser radiations at around 630 nm [DCM (4-(Dicyanomethylene)-2-methyl-6-(4-dimethylaminostyryl)-4*H*-pyran) special] and at around 600 nm (Rhodamine 6G) using an $AgGaS_2$ crystal.[38,39] The

frequencies of both lasers were tuned to achieve the phase matching. The infrared radiation was detected by a liquid N_2 cooled MCT detector. The output power of the infrared radiation generated in a 25 mm long crystal was about 50 μW when pumped by equal-power beams of a total power of 1 W focused by a 10 cm focal length lens. An infrared diode laser spectrometer with a spectral purity of 0.0003 cm^{-1} was also used in the study of the ν_4 band of methane.

The absorption of laser radiation was detected using the tone-burst-type frequency modulation technique[40–42] for higher sensitivity and higher resolution spectroscopy. High power radio frequencies (rf) of 10–300 MHz were mixed with one of the laser radiations in a MgO doped $LiNbO_3$ crystal to produce rf sidebands prior to the generation of infrared radiation. The sidebands were turned on and off at a frequency of about 90 kHz, and the signal was detected by a phase sensitive detector referenced at the burst frequency.

The spectra of methane trapped in solid parahydrogen were recorded separately in Kyoto and in Chicago. The essential features of the spectra observed in the two laboratories were almost the same. The spectra shown in this article are those observed in Kyoto. The spectra observed at Chicago were reported in Ref. 18.

IV. OBSERVED RESULTS

Figure 2 shows the FTIR spectrum of the two infrared active fundamentals of methane in solid parahydrogen at 4.8 K. The upper panel shows the degenerate stretching ν_3 and the lower the degenerate bending ν_4. Part of the spectra were already reported in a previous paper.[19] All the spectral features were reproducible in different samples. The linewidth of the ν_3 transition is about 1 cm^{-1} while that of the ν_4 is about 0.25 cm^{-1}. The latter linewidth is approximately the same as the instrumental limit of the spectrometer, Magna 750. The same sample was also measured by using a difference frequency laser system with a resolution of 0.0001 cm^{-1} to reveal that some of the lines in Fig. 2 (lower panel) are further resolved. As an example, the laser spectrum of the transitions corresponding to the barely resolved peaks at around 1303.7 cm^{-1} (see carefully the slight blunting of the peaks in Fig. 2) are split clearly into a doublet as shown in Fig. 3. The linewidth of the component of the doublet is about 0.027 cm^{-1} (FWHM). In contrast, no further splitting or sharpening was noticed for the ν_3 transition shown in the upper panel of Fig. 2 even at higher resolutions using the difference frequency laser system. The observed frequencies are listed in the first ν_3 and the second ν_4 columns of Table I.

The two spectra in Fig. 2 exhibit four to five fine-structured peaks as denoted by P(1), Q(1), R(0), and R(1), which show a roughly equal spacing of about 8 cm^{-1} for ν_3 and of about 5 cm^{-1} for ν_4. Since these spacings are close to those of the rovibrational transitions of methane in the gas phase, they are assigned to transitions between rotational levels. This assignment is supported by the temporal change of the spectral pattern caused by a slow relaxation of the nuclear spin state of methane and an extensive analysis will be made below.

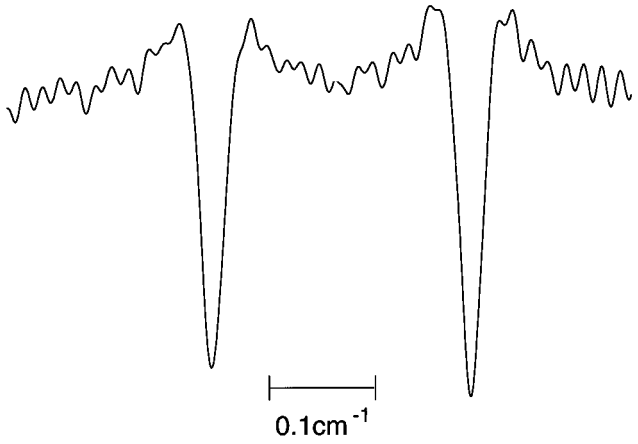

FIG. 3. High resolution laser spectrum of part of the ν_4 transition of methane at 1303.7 cm^{-1} in Fig. 2(b). The spectrum was observed by the tone-burst modulation technique with a rf sideband of 100 MHz. The figure shows that the barely split doublet (actually appearing as a blunted singlet) at around 1303.7 cm^{-1} in Fig. 2(b) consists, in fact, of two lines with linewidths of 0.027 cm^{-1} (FWHM).

V. SPECTRAL ANALYSIS

The four protons in methane couple to give three nuclear spin eigenstates. The states of $I=2$, 1, and 0 are usually designated A, F, and E, respectively.[43,44] Because the nuclear spin statistics require the total wavefunction to be antisymmetric with respect to the interchange of identical protons, combinations of nuclear spin and rotational states are restricted accordingly. For the electronic and vibrational ground state of methane the rotational state of $J=0$ is associated with the nuclear spin state of $I=2$, i.e., the A state, while the state of $J=1$ couples with the F state of $I=1$. As

TABLE I. Observed frequencies, assignments, and polarizations of the ν_3 and ν_4 fundamental bands of methane in solid parahydrogen.

Observed frequencies (cm^{-1})		Assignments	Observed polarization
ν_3	ν_4		
3008.09	1298.21	P(1)	∥
3008.71	1298.85		⊥
	1300.12	?	
3016.33	1302.92	Q(1)	⊥
3016.97	1303.54		∥
3017.54	1303.80		⊥
3025.16	1308.25	R(0)	⊥
3025.94	1308.37		∥
	1309.16		⊥
3030.27	1312.24	R(1)	⊥
3031.02	1312.91		∥
3034.43	1313.55		⊥
	1316.47		
3038.04			⊥
3043.39			
3044.13			
3048.97			

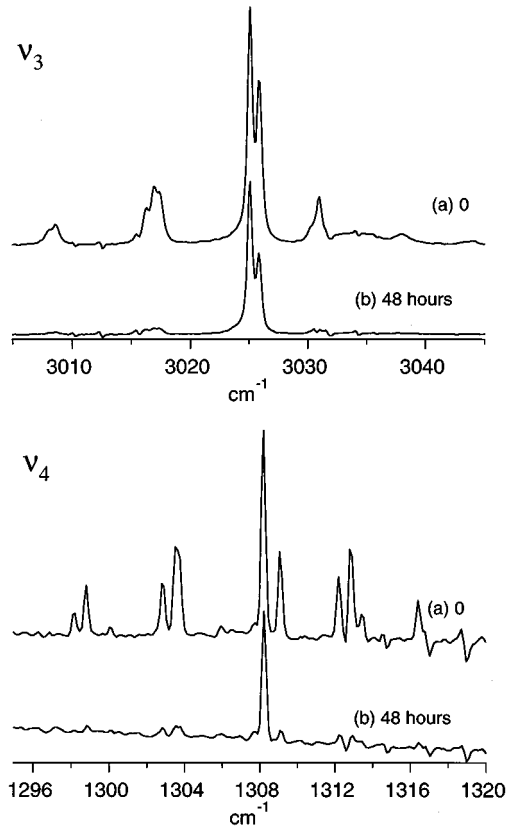

FIG. 4. Temporal dependence of the FTIR spectra of methane trapped in solid parahydrogen. The upper and lower panels show the ν_3 and ν_4 fundamental bands, respectively. In each panel traces (a) and (b) show the spectrum observed immediately after the growth of the crystal and after 48 h standing at 4.8 K, respectively.

for the rotational state of $J=2$, both the E state of $I=0$ and the F state of $I=1$ are possible. Since the transition between different nuclear spin states is forbidden, the population of each rotational level is not determined by the Boltzmann distribution at the cryogenic temperature when the sample gas is cooled quickly from room temperatures to the cryogenic temperature. The rotational population ratio of methane cooled by a supersonic expansion down to about 10 K was reported to be very close to 5:9:2 for $J=0:1:2$, which is the ratio of A, F, and E nuclear spin states at room temperatures.[45]

Although the nuclear spin states are conserved in free space, transitions between different nuclear spin states may be accelerated by nuclear spin-nuclear spin magnetic interaction and spin-rotation interaction.[46–49] In the solid parahydrogen crystal, the magnetic field of impurity orthohydrogen with $J=1$ catalyzes the nuclear spin relaxation. Therefore, it is expected that the population ratio of the nuclear spin states just after the isolation will be close to that for room temperature but that this ratio will gradually approach that corresponding to a Boltzmann distribution equilibrated at 5 K, i.e., $1(J=0):0.1(J=1):0.001(J=2)$. Here, we have assumed a rigid rotor with a rotational constant of $B=5.24\ \mathrm{cm}^{-1}$.

Figure 4 shows the time dependent change of spectral structure for the ν_3 and ν_4 band. In each panel trace (a) is observed immediately after the growth of the crystal while trace (b) is after 48 h. It is seen that all the absorptions except those at 3025.16 cm^{-1} and 3025.94 cm^{-1} in the ν_3 band and at 1308.25 cm^{-1} and 1308.37 cm^{-1} in the ν_4 band disappear almost completely after 48 h. The time dependence clearly indicates that the spectral structure in Fig. 2 is rotational structure dictated by coupling with the nuclear spin states, and the absorptions at 3025.16 cm^{-1}/3025.94 cm^{-1} for ν_3 and at 1308.25 cm^{-1}/1308.37 cm^{-1} for ν_4 are due to transitions starting from the $J=0$ rotational state whereas the diminishing absorptions are due to transitions starting from the $J=1$ and $J=2$ rotational states of the ground vibrational state. Referring to the rotational constants of the gas phase (5.24 cm^{-1}, 5.19 cm^{-1}, and 5.24 cm^{-1} for the ground, the ν_3, and ν_4 excited states, respectively) and the Coriolis coupling constants ($\zeta_3=0.056$, $\zeta_4=0.466$),[50,51] the four groups of peaks can be assigned to P(1), Q(1), R(0), and R(1) transitions, respectively, as designated in Fig. 2 and listed in the third column of Table I. It is to be noted that no absorption from the $J=2$ rotational state was observed although the lowest rotational state coupled with the nuclear spin state of $I=0$ with E symmetry is the $J=2$ state. As mentioned above, the $J=2$ rotational state is coupled not only with the nuclear spin state of $I=0$ but also with the state of $I=1$ with F symmetry. Therefore, relaxation from the nuclear spin state with E symmetry in the $J=2$ rotational state to the $J=1$ rotational state may occur due to the interaction between the nearly degenerate E and F nuclear states in $J=2$, which eventually forces the relaxation from the $J=2$ to $J=1$ rotational state through the channel of the nuclear F state.[46–49] This relaxation might be too fast to permit observation of transitions from the $J=2$ level in our experiment. A quantitative analysis of the nuclear spin conversion will be discussed in a separate article.[52]

The splitting of the order of 0.5 cm^{-1} into doublets or triplets shown in Fig. 2 is due to the crystal field effect. This is substantiated by the agreement between the experimentally observed polarization dependence and the theoretical prediction as discussed in Article I.

Figure 5 shows the polarization dependence of the FTIR spectrum. The upper and lower panels are for the ν_3 and ν_4 bands, respectively. Trace (a) is for the spectrum when the polarization of radiation is parallel to the c axis while trace (b) shows the spectrum for the perpendicular polarization. The polarization dependence was observed by inserting a grid polarizer in front of the crystal. Since there is a slight birefringent effect in the BaF_2 windows, the polarization dependence in Fig. 5 is not perfect but the difference between the two polarizations is evident.

There are two absorptions in the P(1) transition. The transition at lower frequency is for radiation polarized parallel to the c axis, while the higher is for perpendicular polarization. The R(0) transition also shows two peaks. The transition at lower frequency is for perpendicular and that at higher frequency is for parallel polarization. The Q(1) transition consists of three absorptions. The central line is the parallel transition and the others are perpendicular. The polarization dependence as well as the number of absorptions

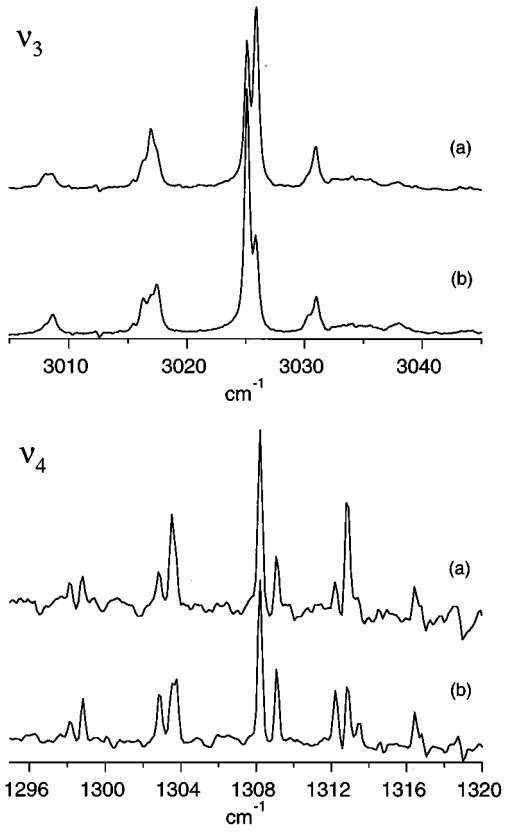

FIG. 5. The polarization dependence of the FTIR spectrum of methane trapped in solid parahydrogen. The upper and lower panels show the ν_3 and ν_4 bands, respectively. In each panel traces (a) and (b) show the spectrum when the polarization of radiation is in parallel with and perpendicular to the c axis, respectively.

in the P(1), Q(1) and R(0) transitions is consistent with the theoretical prediction shown in Fig. 1. The R(1) transition is complicated as discussed in article I. However, the assignment can be made by referring to the calculated transition frequencies from the estimated crystal field parameters discussed in the following. The assignment of the spectrum thus obtained allows us to perform a least squares fitting of the parameters.

According to the theory in Article I, the number of molecular parameters to be determined for the analysis of the spectrum is 13 in total; the rotational constants of the ground (B'') and the excited states (B'_3 and B'_4), the band origins (ν_3 and ν_4), the Coriolis parameters (ζ_3 and ζ_4), and the crystal field parameters of the ground (ϵ''_{3c} and ϵ''_{4c}) and the excited states ($\epsilon'_{3c,3}$, $\epsilon'_{4c,3}$, $\epsilon'_{3c,4}$, and $\epsilon'_{4c,4}$). Since the number of observed transitions is not large enough to determine all the parameters with certainty, it is necessary to reduce somehow the number of the parameters. First, we note that the crystal field parameters ϵ''_{4c}, $\epsilon'_{4c,3}$, and $\epsilon'_{4c,4}$ are not determinable from the observed transitions because of the strong correlation with the other parameters. However, since the effect of the V_4 term of Eq. (1) is relatively small as shown in Article I, the parameter ϵ_{4c} may be assumed to be zero for all the three states. As for the other crystal field parameter ϵ_{3c} in Eq. (1), it is determinable for all the three states, i.e., the ground and the ν_3 and ν_4 excited states. Although the parameter should be different among the three states, the values of ϵ''_{3c}, $\epsilon'_{3c,3}$, and $\epsilon'_{3c,4}$ are found to be accidentally the same within the fitting error despite the fact that they were fitted independently (see caption for Table IV). Therefore, the same value of ϵ_{3c} is assumed for all three states in the fitting. In this way, the total number of the parameters to be fitted was reduced to 8.

To start the numerical fitting it is necessary to have an initial value of the crystal field parameter ϵ_{3c}. The search for the initial value was conducted as follows: According to the theory[33] the $J=1$ level of the ground vibrational state is to split into two and the EF_2 state is to come below the A_2F_1 state (see Fig. 1). This theoretical prediction is confirmed by the observed polarization dependence of the P(1) transition as shown in Fig. 5, and the splitting is found experimentally to be 0.64 cm^{-1}. Using only the first V_3 term of the crystal field in Eq. (1), the theoretical splitting is approximated by $-2B''+\sqrt{4B''^2+(5/98)\epsilon''^2_{3c}}$ where B'' and ϵ''_{3c} are the rotational constant and the crystal field parameter of the ground state to be determined, respectively.[33] If the gas phase rotational constant of 5.24 cm^{-1} is adopted, the approximate absolute value of the crystal field parameter is calculated as 16.5 cm^{-1}. Since the sign of the parameter is predicted to be negative,[33] the initial guess for the crystal field parameter of the ground state is thus determined to be $\epsilon_{3c}=-16.5\ \mathrm{cm}^{-1}$.

Using this initial crystal field parameter, the observed transition frequencies were fitted by the standard method of the least squares fitting. The result of the fitting is given in Tables II and III along with the observed frequencies for the ν_3 and ν_4 transitions, respectively. The first and second columns of the tables list the observed frequencies and the polarization dependence, the third the assignments of the transitions, the fourth and fifth columns demonstrate the calculated frequencies and the difference between the observed and calculated frequencies. The last column shows the predicted polarization dependence. The molecular parameters deduced from the spectral data are summarized in Table IV along with the gas phase values.

Considering the fact that the accuracy of the observed frequencies is limited by the resolution of the FTIR spectrometer we used, that is 0.25 cm^{-1}, the agreement between the observed and calculated transition frequencies is quite satisfactory. The relatively poor agreement of the two transitions of R(1) of ν_3 at 3038.04 and 3048.97 cm^{-1} is attributed to the uncertainty of the observed frequencies due to the broader and weaker absorption peaks.

At this point, it may be helpful to explain a little more our assignment of the complicated R(1) transitions: The transitions at 3030.27, 3031.02, and 3034.43 cm^{-1} of ν_3 are easily assigned to the strongly allowed transitions obeying the $\Delta R=0$ selection rule, while the relatively weak transitions at 3038.04, 3043.39, and 3044.13 cm^{-1} are associated with the $\Delta R\neq 0$ forbidden transitions. The highest frequency transition at 3048.97 cm^{-1} is attributed to the $\Delta R\neq 0$ forbidden transitions from $J=0$ rotational level of the ground vibra-

TABLE II. The observed frequencies, the assignments, and the calculated frequencies of the ν_3 transition of methane in solid parahydrogen.

Observed		Calculated									
		Assignments									
		Upper state				Lower state					
Frequencies (cm^{-1})	Polarization	J'	R'	M'	Γ'	J''	M''	Γ''	Frequencies (cm^{-1})	Obs.-calc.	Predicted polarization	
3008.09	∥	0	1	0	$A_1\overline{F_2}$	1	0	$A_2\overline{F_1}$	3008.13	−0.04	∥	
3008.71	⊥	0	1	0	A_1F_2	1	±1	EF_2	3008.80	−0.09	⊥	
3016.33	⊥	1	1	±1	EF_1	1	0	A_2F_1	3016.18	0.15	⊥	
3016.97	∥	1	1	±1	EF_1	1	±1	EF_2	3016.85	0.12	∥	
3017.54	⊥	1	1	0	A_2F_2	1	±1	EF_2	3017.49	0.05	⊥	
		1	2	±1	EF_2	1	±1	EF_2	3017.56	−0.02	⊥	*
3025.16	⊥	1	0	±1	EA_1	0	0	A_1A_1	3025.31	−0.15	⊥	
3025.94	∥	1	0	0	A_2A_2	0	0	A_1A_1	3025.90	0.04	∥	
3030.27	⊥	2	1	±1	EF_1	1	0	A_2F_1	3030.42	−0.15	⊥	
3031.02	∥	2	1	±1	EF_1	1	±1	EF_2	3031.09	−0.07	∥	
		2	1	±2	EF_2	1	±1	EF_2	3031.12	−0.10	⊥	
		2	1	0	A_1F_2	1	0	A_2F_1	3033.95	-	∥	
3034.43	⊥	2	1	0	A_1F_2	1	±1	EF_2	3034.62	−0.19	⊥	
		2	2	±2	EF_1	1	0	A_2F_1	3035.45	-	⊥	*
		2	2	±2	EF_1	1	±1	EF_2	3036.12	-	∥	*
		2	3	0	A_1F_2	1	0	A_2F_1	3036.92	-	∥	*
3038.04	⊥	2	2	±1	EF_2	1	±1	EF_2	3038.79	−0.75	⊥	*
3043.39		2	3	±1	EF_1	1	0	A_2F_1	3043.57	−0.18	⊥	*
3044.13		2	3	±2	EF_2	1	±1	EF_2	3044.26	−0.13	⊥	*
3048.97		2	3	±2	EA_1	0	0	A_1A_1	3048.71	0.26	⊥	*

The asterisk in the last column shows the transition of $\Delta R \neq 0$.

tional state by referring to the energy diagram in Fig. 1. Beyond this point, however, we are unable to assign the weak absorption at 3030–3048 cm^{-1} in Fig. 2 in relation to the many forbidden transitions marked by asterisks in Table II and by small solid circles in Fig. 1 because it is difficult to identify the broad absorption in this region.

As for the ν_4 transition, those at 1312.24, 1312.91, 1313.55, and 1316.47 cm^{-1} are assigned to the $\Delta R=0$ ''allowed'' transitions. As predicted in Article I, the $\Delta R \neq 0$ transitions are weaker in the ν_4 transition than in the ν_3. The transition at 1309.16 cm^{-1} is the only $\Delta R \neq 0$ transition detected.

TABLE III. The observed frequencies, the assignments, and the calculated frequencies of the ν_4 transition of methane in solid parahydrogen.

Observed		Calculated									
		Assignments									
		Upper state				Lower state					
Frequencies (cm^{-1})	Polarization	J'	R'	M'	Γ'	J''	M''	Γ''	Frequencies (cm^{-1})	Obs.-calc.	Predicted polarization	
1298.21	∥	0	1	0	$A_1\overline{F_2}$	1	0	$A_2\overline{F_1}$	1298.25	−0.04	∥	
1298.85	⊥	0	1	0	A_1F_2	1	±1	EF_2	1298.92	−0.07	⊥	
1302.92	⊥	1	1	±1	EF_1	1	0	A_2F_1	1302.78	0.14	⊥	
1303.54	∥	1	1	±1	EF_1	1	±1	EF_2	1303.45	0.09	∥	
1303.80	⊥	1	1	0	A_2F_2	1	±1	EF_2	1303.72	0.08	⊥	
1308.25	⊥	1	0	0	EA_1	0	0	A_1A_1	1308.31	−0.06	⊥	
1308.37	∥	1	0	±1	A_2A_2	0	0	A_1A_1	1308.43	−0.06	∥	
1309.16	⊥	1	2	±1	EF_2	1	±1	EF_2	1309.09	0.07	⊥	*
1312.24	⊥	2	1	±1	EF_1	1	0	A_2F_1	1312.27	−0.03	⊥	
1312.91	∥	2	1	0	A_1F_2	1	0	A_2F_1	1312.87	0.04	∥	
		2	1	±1	EF_1	1	±1	EF_2	1312.94	−0.03	∥	
1313.55	⊥	2	1	0	A_1F_2	1	±1	EF_2	1313.54	0.01	⊥	
1316.47		2	1	±2	EF_2	1	±1	EF_2	1316.61	−0.14	⊥	

The asterisk in the last column shows the transition of $\Delta R \neq 0$.

TABLE IV. The optimized molecular parameters.

	Solid hydrogen	Gas phase
Ground state		
B''	4.793 (42)	5.241
ν_3 Excited state		
ν_3	3017.26 (11)	3019.491
B_3'	4.603 (18)	5.192
ζ_3	0.0450 (51)	0.0558
ν_4 Excited state		
ν_4	1303.62 (11)	1310.761
B_4'	4.591 (40)	5.240
ζ_4	0.4654 (56)	0.4664
Crystal field		
ϵ_{3c}	−25.80 (37)	0.0
ϵ_{4c}	0.0 (fixed)	0.0

The rotational constant B, the band origin ν, and the crystal field parameters (ϵ_{3c} and ϵ_{4c}) of the ground and the ν_3 and ν_4 excited states are in units of cm^{-1} except for the Coriolis parameter ζ. Uncertainty in parentheses are one standard deviation in the last figure quoted. The gas phase values in the last column are taken from Refs. 50 and 51. The crystal field parameter ϵ_{3c} is assumed to be the same for the ground and the excited vibrational states. The value of ϵ_{4c} is fixed to 0.0 in the calculation (see text). When the crystal field parameters ϵ_{3c} is fitted independently for the three states, the optimized values are found to be $\epsilon_{3c}''=-23.6$ (22), $\epsilon_{3c,3'}=25.35$ (48), and $\epsilon_{3c,4'}=-24.6$ (13) for the ground and the ν_3 and ν_4 excited states, respectively, resulting in slight changes of the other molecular parameters but within the standard deviation as listed above.

It should be remembered that the number of observable transitions is limited because of the narrow range of the temperature of the system so that transitions from $J>1$ are not observable. This limitation entails uncertainty in the parameter fitting. However, in spite of this limitation the present work demonstrates that the quantitative spectral analysis of a system in parahydrogen crystal is feasible in the rovibrational regime.

VI. DISCUSSION

A. Rotational constants and Coriolis coupling constants

From Table IV we see that the rotational constants of methane in solid parahydrogen are about 10% smaller than those in the free space. The increase of the effective mass of methane in the crystal due to the molecular interaction accounts for the decrease of the rotational constants. To be more precise, the rotational constants of the excited states are about 12% smaller, while that of the ground state is smaller by 9.6%. The larger degree of reduction of the constants in the former suggests that the isotropic interaction between methane and the surrounding hydrogen molecules is stronger in the vibrationally excited state than in the ground state.

The modified Coriolis parameters for both ν_3 and ν_4 states are almost the same as the gas phase values. This shows that the coupling between the vibration and the rotation of methane in the solid are almost the same as in the gas phase. In other words, it may well be considered that methane rotates almost freely in solid parahydrogen.

B. Molecular interactions and crystal field

Although we assumed that the crystal field parameter ϵ_{3c} was the same in the ground and in the two excited vibrational states, the fitting of the spectrum is quite satisfactory as shown in Tables II and III. The result leads to the conclusion that the difference of the parameter among these states is small or is not large enough to be detected by the present spectral resolution.

As shown in Table IV the final crystal field parameter ϵ_{3c} assumed to be common is calculated to be -25.80 ± 0.37 cm^{-1} which is comparable with the theoretically predicted value of -19.24 cm^{-1} in Article I. Further improvement in the theoretical value may be attainable if proper account is taken of the following three points. First, in the calculation of the crystal sum we have assumed that the hydrogen molecules are at the equilibrium position of $R=3.783$ Å. However, since the mean amplitude of the zero-point vibration amounts to almost 20% of the intermolecular distance, the effect of the expansion of the molecular wavefunction due to the large amplitude should be included. This is the so-called phonon renormalization problem.[16] Secondly, the assumption that the crystal field effect is additive means that we neglect the effect of many body interactions such as the three body interaction. The inclusion of this effect should improve the agreement between theory and experiment. Finally, the use of the London formula for estimation of the value of ϵ_{3c}[33] is, perhaps, too crude. A dependable *ab initio* calculation of the anisotropic potential should provide a better estimation of the crystal field parameter.

From the experimentally determined crystal field parameter of $\epsilon_{3c}=-25.80$ cm^{-1} the expansion coefficient A_3 of the third order dispersion interaction between methane and a parahydrogen molecule with $J=0$ in

$$V(\omega_{CH_4};R)=A_3(R)\frac{i}{\sqrt{2}}[D^{(3)}_{2,0}(\omega_{CH_4})-D^{(3)}_{-2,0}(\omega_{CH_4})]$$

is calculated to be $A_3(R_0)=34.49$ cm^{-1} at $R_0=3.783$ Å where ω_{CH_4} is the orientation of methane relative to the intermolecular axis. Since the phonon renormalization effect is neglected in the calculation, the value may be slightly overestimated.

C. Linewidth

Typical linewidths of the ν_4 transitions in the high resolution laser spectrum are 0.027 cm^{-1} (FWHM) as shown in Fig. 2 while those of ν_3 transitions are about 1 cm^{-1} (FWHM). The difference in linewidth between the ν_3 and ν_4 transitions suggests that the phonon couples more strongly with the stretching vibration of ν_3 than with the bending vibration of ν_4. Since the ν_3 triply degenerate stretching mode changes the instantaneous molecular size upon vibration much more significantly than does the ν_4 bending mode, a stronger coupling between the ν_3 vibrationally excited state and the lattice vibration is conceivable, that is to say, the

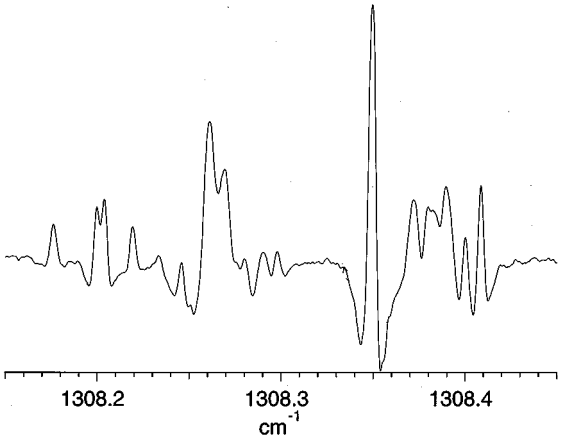

FIG. 6. High resolution spectrum of the R(0) band at 1308.25 and 1308.37 cm^{-1} in Fig. 1. The spectrum was observed after a prolonged standing beyond 48 h. The tone-burst modulation technique with a rf sideband of 60 MHz was applied. The linewidth is as narrow as 0.003 cm^{-1} (100 MHz).

phonon assisted relaxation of the $v=1$ excited state may be more efficient in the ν_3 than in the ν_4 mode. Further quantitative analysis is desired in this respect.

D. Interaction between an orthohydrogen and a methane molecule

The singlet like R(0) transition of the ν_4 shown in Fig. 4(b) is found to show further splitting by high resolution spectroscopy. Figure 6 shows a part of the R(0) transition recorded several days after the preparation of the crystal by using the difference frequency laser (see Sec. III). The transition consists of more than 20 sharp lines with linewidths as narrow as 0.003 cm^{-1} (100 MHz). Since these linewidths are almost one order of magnitude sharper than those of the rotational branches of the ν_4 transition in Fig. 2, the spectral structure in Fig. 6 must arise from some different physical origin. Since the spectrum in Fig. 6 is completely different from the spectrum of methane cluster reported in a separate article,[53] the spectral structure in Fig. 6 is regarded as due to the isolated monomeric methane in solid parahydrogen.

These spectral structures are considered to be due to the interaction between methane and the residual orthohydrogen with $J=1$ in the crystal. The orthohydrogen molecule may be a mobile species even at low temperatures by means of rotational diffusion or quantum diffusion.[16] Since the orthohydrogen has a permanent quadrupole moment, the interaction between methane and orthohydrogen should be stronger than the interaction between methane and parahydrogen. When orthohydrogen reaches methane as the nearest neighbor, the pair state is stabilized and the rotational diffusion ceases. Therefore, the number of pairs of methane and orthohydrogen will increase with time. Such a pair state is described by a product of the rotational wavefunctions of methane and orthohydrogen. The degeneracy of the rotational wavefunction of methane and of the magnetic quantum number m of orthohydrogen ($m=0,\pm1$) is lifted by both the intermolecular interaction and the crystal field. Since the quantization axis in this case is along the pair axis, the in-plane pair and the out-of-plane pair should lead to different energy levels as in the case of deuterium orthohydrogen pairs in the parahydrogen crystal.[14] As a result of this pairwise interaction, more than 20 lines are expected. Detailed analysis of this pair state is under study.

VII. CONCLUSION

In this article we have analyzed the rovibrational levels of methane trapped in a solid parahydrogen crystal. The analysis indicates that methane occupies a substitutional site and that the crystal symmetry surrounding methane is not perturbed by the substitution. The theoretically predicted spectrum agrees satisfactorily with the experimental in all aspects. Quantitative agreement of the rovibrational frequencies is obtained by taking into account the crystal field effect properly. No significant difference of the crystal field parameters for the ground and the excited vibrational states is found, and the common value is determined to be -25.80 ± 0.37 cm^{-1} for ϵ_{3c}. The experimentally determined crystal field parameter of the ground state is in fair agreement with the theoretical value. From the observed crystal field parameter the pair potential between methane and hydrogen molecules is evaluated to be $A_3(R_0)=34.49$ cm^{-1} at $R_0=3.783$ Å under the assumption that the phonon renormalization effect is negligibly small. If a value of A_3 is given by some means for a pair of methane and hydrogen molecules in the gas phase, the difference between the gaseous value and the present values will provide information on the effect of phonon renormalization in quantum solids.

In conclusion, the present work strongly demonstrates that solid parahydrogen is a powerful matrix for the study of intermolecular interactions and eigenstates of molecules in the solid matrix.

Note added in proof. After the submission of our paper we were informed that Fajardo and his co-workers observed the rotationally resolved CH_4 spectrum in parahydrogen matrix by laser ablation of graphite [S. Tam, M. Macler, and M. E. Fajardo, J. Chem. Phys. **106**, 8955 (1997)].

ACKNOWLEDGMENTS

The authors are grateful to Professor Eizi Hirota for his continuing interest in the present work. The work in Kyoto was financially supported by the Grant-in-Aid for Scientific Research of the Ministry of Education, Science, Culture, and Sports of Japan. The Chicago group was supported by the Air Force Grant No. 49620-94-1-0145. T.M. acknowledges financial support from the Kurata Foundation, the Matuo Foundation, the Japan Securities Scholarship Foundation, and the Research Foundation for Opto-Science and Technology.

[1] See for example, *Laser Spectroscopy of Solids*, edited by W. M. Yen and P. M. Selzer, Topics in Applied Physics, Vol. 49 (Springer-Verlag, Berlin, 1986).
[2] M. Okumura, M.-C. Chan, and T. Oka, Phys. Rev. Lett. **62**, 32 (1989).
[3] T. Oka, Annu. Rev. Phys. Chem. **44**, 299 (1993).

[4] D. P. Weliky, T. J. Byers, K. E. Kerr, T. Momose, R. M. Dickson, and T. Oka, Appl. Phys. B **59**, 265 (1994).
[5] M.-C. Chan, M. Okumura, C. M. Gabrys, L.-W. Xu, B. D. Rehfuss, and T. Oka, Phys. Rev. Lett. **66**, 2060 (1991).
[6] M.-C. Chan, S. S. Lee, M. Okumura, and T. Oka, J. Chem. Phys. **95**, 88 (1991).
[7] M.-C. Chan, L.-W. Xu, C. M. Gabrys, and T. Oka, J. Chem. Phys. **95**, 9404 (1991).
[8] T. Momose, D. P. Weliky, and T. Oka, J. Mol. Spectrosc. **153**, 760 (1992).
[9] R. A. Steinhoff, K. V. S. R. Apparao, D. W. Ferguson, K. N. Rao, B. P. Winnewisser, and M. Winnewisser, Can. J. Phys. **72**, 1122 (1994).
[10] R. A. Steinhoff, B. P. Winnewisser, and M. Winnewisser, Phys. Rev. Lett. **73**, 2833 (1994).
[11] K. E. Kerr, T. Momose, D. P. Weliky, C. M. Gabrys, and T. Oka, Phys. Rev. Lett. **72**, 3957 (1994).
[12] R. M. Dickson, T. J. Byers, K. E. Kerr, and T. Oka, J. Low Temp. Phys. **102**, 241 (1996).
[13] T. Momose, T. Wakabayashi, and T. Shida, Czech. J. Phys. **46**, 529 (1996).
[14] D. P. Weliky, K. E. Kerr, T. J. Byers, Y. Zhang, T. Momose, and T. Oka, J. Chem. Phys. **105**, 4461 (1996).
[15] I. F. Silvera, Rev. Mod. Phys. **52**, 393 (1980).
[16] J. van Kranendonk, *Solid Hydrogen* (Plenum, New York, 1983).
[17] P. C. Souers, *Hydrogen Properties for Fusion Energy* (University of California Press, Berkeley, 1986).
[18] M.-C. Chan, Ph. D. thesis, The University of Chicago, 1991.
[19] T. Momose, M. Miki, M. Uchida, T. Shimizu, I. Yoshizawa, and T. Shida, J. Chem. Phys. **103**, 1400 (1995).
[20] T. Momose, M. Uchida, N. Sogoshi, M. Miki, S. Masuda, and T. Shida, Chem. Phys. Lett. **246**, 583 (1995).
[21] M. Miki, T. Wakabayashi, T. Momose, and T. Shida, J. Phys. Chem. **100**, 12 135 (1996).
[22] N. Sogoshi, T. Wakabayashi, T. Momose, and T. Shida, J. Phys. Chem. **101**, 522 (1997).
[23] L. Pauling, Phys. Rev. **36**, 430 (1930).
[24] A. Cabana, G. B. Savitsky, and D. F. Horning, J. Chem. Phys. **39**, 2942 (1963).
[25] F. H. Frayer and G. E. Ewing, J. Chem. Phys. **48**, 781 (1968).
[26] A. Chamberland, R. Belzile, and A. Cabana, Can. J. Chem. **48**, 1129 (1970).
[27] B. Nelander, J. Chem. Phys. **82**, 5340 (1985).
[28] L. H. Jones, S. A. Ekberg, and B. I. Swanson, J. Chem. Phys. **85**, 3203 (1986).
[29] L. H. Jones and S. A. Ekberg, J. Chem. Phys. **87**, 4368 (1987).
[30] M. Prager, B. Asmussen, W. Langel, C. J. Carlile, and H. Blank, J. Chem. Phys. **99**, 2052 (1993).
[31] M. Prager, B. Asmussen, and C. J. Carlile, J. Chem. Phys. **100**, 247 (1994).
[32] R. E. Miller and J. C. Decius, J. Chem. Phys. **59**, 4871 (1973).
[33] T. Momose, J. Chem. Phys. **107**, 7695 (1997), preceding paper.
[34] J. T. Hougen, *International Review of Science, Physical Chemistry*, Ser. 2, Vol. 3, Spectroscopy, edited by D. A. Ramsay (Butterworths, London, 1976) pp. 75–125.
[35] L. D. Landau and E. M. Lifshitz, *Quantum Mechanics: Non-Relativistic Theory*, 3rd edition (Pergamon, New York, 1977), for example.
[36] K. T. Hecht, J. Mol. Spectrosc. **5**, 355 (1960).
[37] A. Pine, J. Opt. Soc. Am. **64**, 1683 (1974); **66**, 97 (1976).
[38] P. Canarelli, Z. Benko, R. Curl, and F. K. Tittel, J. Opt. Soc. Am. B **9**, 197 (1992).
[39] A. H. Hielscher, C. E. Miller, D. C. Bayard, U. Simon, K. P. Smolka, R. Curl, and F. K. Tittel, J. Opt. Soc. Am. B **9**, 1962 (1992).
[40] H. M. Pickett, Appl. Opt. **19**, 2745 (1980).
[41] C. S. Gudeman, M. H. Begemann, J. Pfaff, and R. J. Saykally, Opt. Lett. **8**, 310 (1983).
[42] H. Adams, J. L. Hall, R. F. Curl, J. V. V. Kasper, and F. K. Tittel, J. Opt. Soc. Am. B **1**, 710 (1984).
[43] E. B. Wilson, J. Chem. Phys. **3**, 276 (1933).
[44] G. Herzberg, *Molecular Spectra and Molecular Structure II, Infrared and Raman Spectra of Polyatomic Molecules* (Krieger, Florida, 1991).
[45] M. Hepp, G. Winnewisser, and K. M. T. Yamada, J. Mol. Spectrosc. **164**, 311(1994).
[46] R. F. Curl, Jr., J. V. V. Kasper, and K. S. Pitzer, J. Chem. Phys. **46**, 3220 (1966).
[47] P.-N. Yi, I. Ozier, and C. H. Anderson, Phys. Rev. **165**, 92 (1968).
[48] I. Ozier, P.-N. Yi, A. Khosla, and N. F. Ramsay, Phys. Rev. Lett. **24**, 642 (1970).
[49] J. T. Hougen, J. Chem. Phys. **55**, 1122 (1971).
[50] J. Susskind, J. Mol. Spectrosc. **45**, 457 (1973).
[51] A. G. Robiette, J. Mol. Spectrosc. **86**, 143 (1981).
[52] T. Miki, T. Momose, and T. Shida (unpublished).
[53] T. Momose, H. Katsuki, H. Hoshina, N. Sogoshi, T. Wakabayashi, and T. Shida, J. Chem. Phys. **107**, 7717 (1997), following paper.